JOURNAL OF MATERIALS SCIENCE 21 (1986) 547–558

Annealing kinetics of cold-rolled plain carbon steels

D. T. GAWNE
Department of Materials Technology, Brunel University, Uxbridge UB8 3PH, UK
G. M. H. LEWIS
Welsh Laboratory, Corporate R & D, British Steel Corporation, Port Talbot, UK

Softening of rimmed steel during batch annealing is due to recrystallization, grain growth and carbide coarsening. The post-recrystallization softening process is used commercially to control product quality and its kinetics can be characterized by an apparent activation energy. This parameter is shown to increase with decreasing carbon content owing to the influence of carbide particle dissolution on the grain growth rate. The latter effect is suppressed by low manganese and high sulphur contents because of the formation of fine manganese sulphide precipitates. The apparent activation energy of softening can be applied to improve the economics of industrial batch annealing.

1. Introduction

It is impracticable to achieve satisfactory gauge and shape control in wide strip with thicknesses below about 1.6 mm on conventional continuous hot mills. The large-scale demand for thinner strip (e.g. 0.8 mm for car bodies) is met by cold rolling. Cold rolling, however, generates a hard, brittle material and annealing is required to restore the ductility. Softening during annealing takes place in two distinct stages: recrystallization and microstructural coarsening. Recrystallization removes the dislocation substructure and operates at a relatively rapid rate (e.g. ~0.5 min at 700° C). However, recrystallization alone does not provide the high level of a formability required by the steel user and continued annealing is necessary. The continued annealing produces further softening by coarsening the constituent particles and grains; this post-recrystallization process can be described generally as microstructural coarsening.

The most commonly used production annealing process is at present batch annealing, in which tightly wound coils of strip steel are stacked in a furnace prior to firing. Microstructural coarsening proceeds at a much slower rate than recrystallization, and a further 20 to 30 h of annealing time after recrystallization is commonly given in commercial batch-annealing cycles. This slow rate of softening enables the microstructural coarsening stage to be used as a control variable in annealing. The soak time and temperature of annealing play an important role in fixing the quality and price of the finished product.

Softening is a thermally activated process, the rate of which depends upon the time and temperature of the anneal and the metallurgical characteristics of the material. Hudd [1] has derived a rate equation expressing the amount of softening in terms of time and temperature of annealing for a rimmed steel. The latter study, however, did not deal with the effects of compositional and process variables, and the present paper concentrates on the influence of these variables on softening by microstructural coarsening.

2. Experimental procedure

Samples were taken from a large number of production hot-rolled coils and, after chemical analysis, six materials with the appropriate compositions (Table I) were selected for further study. The production hot-rolling conditions consisted of slab reheating at about 1300° C, finishing at 900° C and coiling at 600° C. The hot finished samples (2 mm in thickness) were then cold-reduced by 60% with lubrication and heavy reductions per pass on a laboratory mill. Simulated batch annealing was carried out under a nitrogen–hydrogen atmosphere by using a heating rate of 30° C h^{-1} to a specified annealing temperature, and cooling to 150° C in about 60 h with the cooling rate progressively decreasing with falling temperature. Five annealing temperatures between 635° and 715° C, with ten soaking times between 0.1 and 75 h at each temperature, were used for each steel.

The influence of hot-rolled structure and cold reduction on softening kinetics were investigated using Steel A, since this had a composition typical of an extra deep drawing (EDD or CR2 grade) rimmed steel. A series of heat treatments on the hot rolled samples of

TABLE I Compositions of steels

Steel	Elemental composition (wt %)				
	C	Mn	S	P	N
A	0.056	0.34	0.022	0.007	0.0030
B	0.055	0.32	0.039	0.014	0.0046
C	0.024	0.21	0.017	0.011	0.0032
D	0.028	0.33	0.019	0.008	0.0026
E	0.097	0.33	0.033	0.007	0.0032
F	0.098	0.33	0.033	0.014	0.056

0022–2461/86 $03.00 + .12

TABLE II Effect of composition on as-recrystallized grain size* (coiling temperature 600° C, cold reduction 60%)

Steel	Grain intercept length (mm)
A	0.0083
B	0.0077
C	0.0085
D	0.0093
E	0.0073
F	0.0070

Steel A showed that 12 h at 750° C followed by furnace-cooling gave a similar microstructure in terms of carbide morphology and grain structure to that of a steel of very similar composition hot-rolled in production and coiled at 750° C. The latter laboratory treatment was taken as a simulation of a high coiling temperature on Steel A, and the resulting material was designated A(HCT). Samples of A(HCT) were then cold rolled by 60% and given the above annealing cycles. The influence of cold reduction on properties was studied by cold rolling the production as-hot rolled samples of Steel A by 45, 60 and 70% on a laboratory mill prior to annealing. These materials are designated A(45CR), A(60CR) and A(70CR) respectively.

Grain sizes and carbide spacings were determined by the linear intercept method. Hardness measurements (Rockwell R30T) were carried out on strips cut perpendicular to the rolling direction. Recrystallization was followed by hardness measurements on samples removed from the furnace and air-cooled during the heating stage of a simulated batch anneal.

3. Results

3.1. Recrystallization

The start temperature for recrystallization of the various steels lay in the range 505 to 520° C and the finish temperatures 570 to 585° C during the heating stage of batch annealing (Fig. 1a). Steel E recrystallizes first and its relatively fine as-recrystallized grain structure (Table II) suggests a high nucleation rate of recrystallization due to its high carbon and thus cementite content, resulting in extensive particle-aided nucleation of recrystallized grains [2, 3].

The influence of process variables on recrystallization temperature was investigated using Steel A. The use of a high simulated coiling temperature (~ 750° C) increased the recrystallization start temperature by about 5° C (Fig. 1b); this is most likely due to the reduction in nucleation site area per unit volume caused by carbide and grain coarsening. Raising the cold reduction from 45 to 70% resulted in a decrease of 10° C in the recrystallization temperature, the greater difference occurring between 45 and 60% (Fig. 1b). Although an increase in deformation is expected to raise both the nucleation and growth rate of

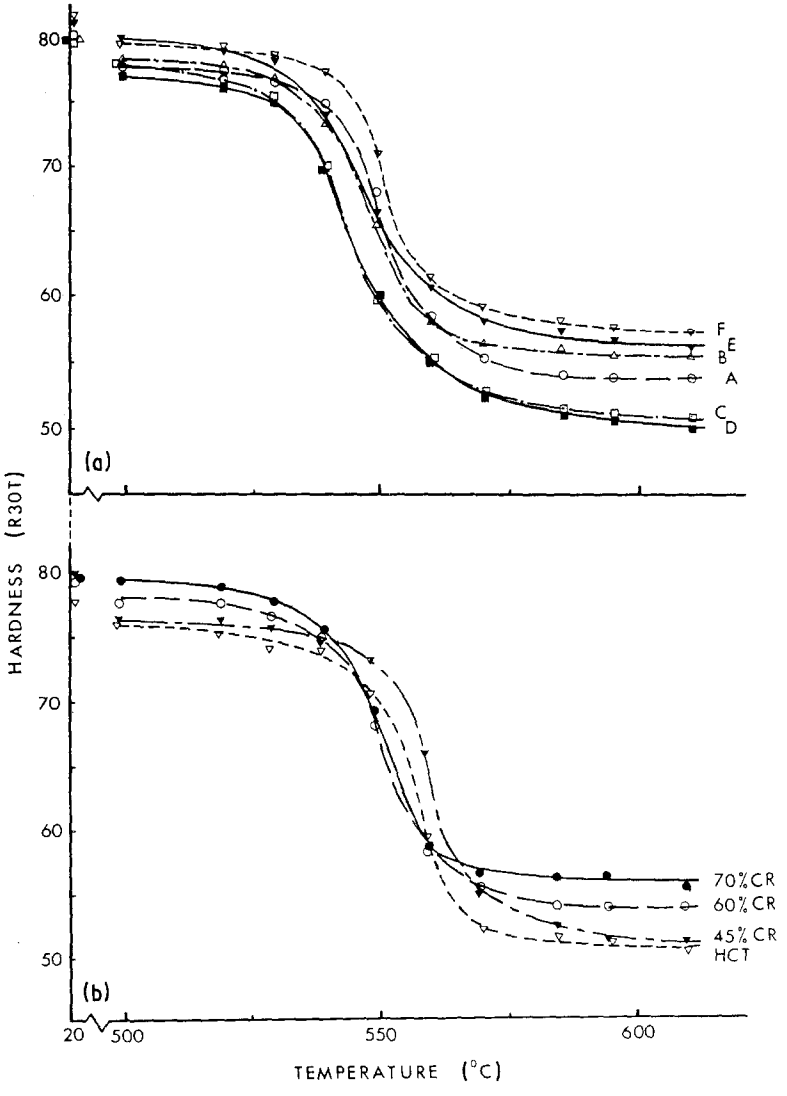

Figure 1 (a) Effect of composition on recrystallization (all steels cold reduced by 60%); (○) Steel A, (△) Steel B, (□) Steel C, (■) Steel D, (▼) Steel E, (▽) Steel F. (b) Effect of processing on Steel A; (▼) cold reduction 45%, coiling temperature 600° C; (○) 60%, 600° C; (●) 70%, 600° C; (▽) 60%, 750° C.

TABLE III Effect of process variables on Steel A

Coiling temperature (° C)	Cold reduction (%)	Grain intercept length (mm)
750	60	0.0089
600	45	0.0102
600	60	0.0083
600	70	0.0068

*The as-recrystallized grain sizes were measured from materials removed from the furnace at 585° C during the heating part of the annealing cycle.

recrystallization, it is found to refine the grain structure (Table III) implying that the nucleation effect predominates. In conclusion, the normal compositional and process variations have relatively small effects on the recrystallization temperature of rimmed steel.

3.2. Microstructural coarsening

Softening of the steels in the microstructural coarsening stage of annealing was followed by hardness measurements. The hardness H of each steel was shown to decrease linearly with the logarithm of the soaking time t at a given annealing temperature, as shown in Fig. 2. The gradients of these hardness–time plots at a given hardness level gave the rates of softening dH/dt, which were found to conform with the Arrhenius relationship over the commercial batch annealing soak temperature range, 650 to 715° C:

$$dH/dt = A \exp(-Q/RT) \quad (1)$$

where Q is the activation energy for softening, T the absolute temperature (K) and R the universal gas constant. Taking logarithms of Equation 1,

$$\log\left(\frac{dH}{dt}\right) = \log A - \frac{Q}{2.303RT} \quad (2)$$

TABLE IV Effect of composition on apparent activation energies of softening and relative softening rates (coiling temperature 600° C, cold reduction 60%)

Steel	Apparent activation energy (kJ mol^{-1})	Softening rate relative to that at 660° C	
		715° C	620° C
A	370	15.0	0.12
B	280	7.3	0.21
C	320	10.2	0.15
D	490	33	0.06
E	250	5.9	0.24
F	280	7.6	0.20

The apparent activation energy Q indicates the sensitivity of the softening rate to temperature. The magnitude of Q can be determined from the gradient of a plot of the logarithm of the softening rate against the reciprocal of the annealing temperature. An approximate value of Q is first derived from a plot of hardness against soaking time. This value is then used to correct the results for the additional softening taking place during the heating and cooling stages of the annealing cycle, by integrating over the time–temperature trace. A more accurate value of Q can then be calculated and, if necessary, the correction procedure can be repeated to increase the accuracy further. The data in Fig. 2 are corrected for the additional softening occurring during the heating and cooling stages.

The calculated values of the apparent activation energies for the steels range from 250 kJ mol^{-1} for Steel E to 490 kJ mol^{-1} for Steel D (Table IV). Hudd [1] used tensile strength instead of hardness to follow softening and obtained an apparent activation energy of 330 kJ mol^{-1} for a steel containing 0.04 wt % carbon, 0.02 wt % sulphur, 0.33 wt % manganese and 0.0034 wt % nitrogen and processed under the same conditions as the steels in the current investigation.

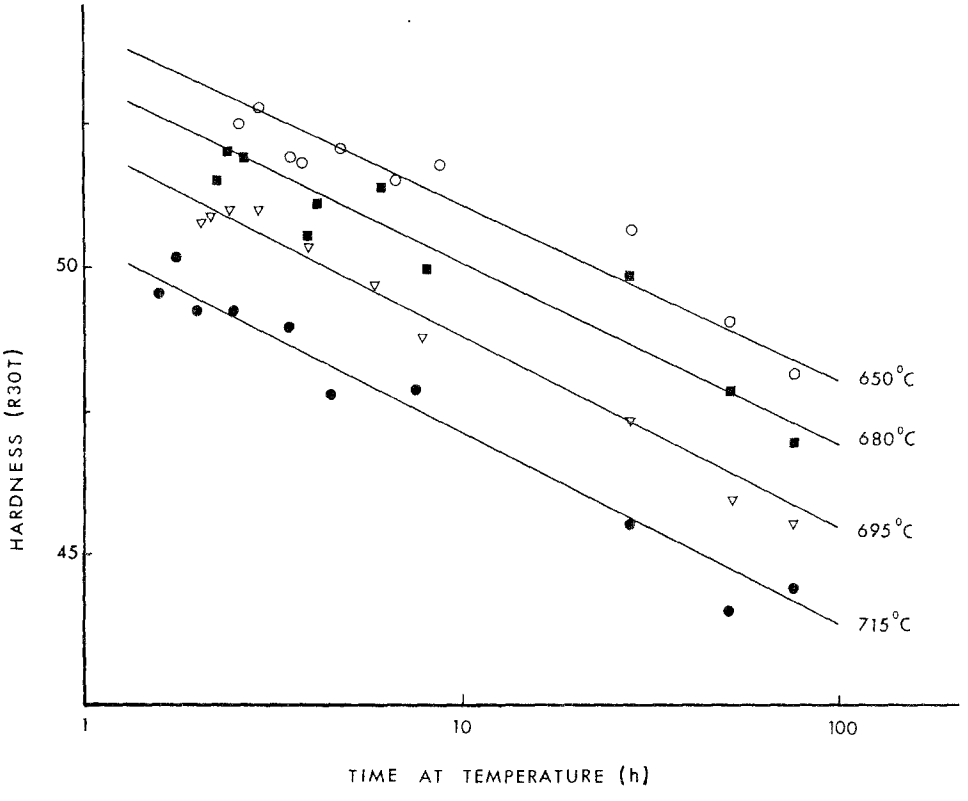

Figure 2 Hardness of Steel A (coiled at 600° C, cold reduced by 60%) as a function of time at various annealing temperatures: (○) 650° C, (■) 680° C, (▽) 695° C, (●) 715° C.

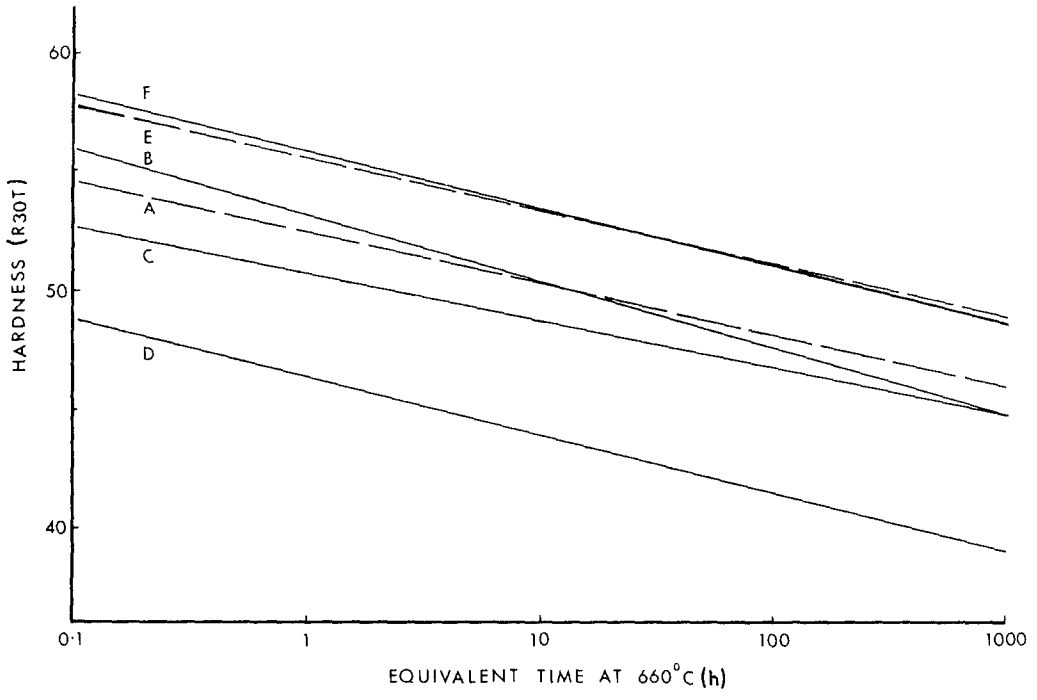

Figure 3 Hardness of annealed steels (coiled at 600°C, cold reduced by 60%) against equivalent time at 660°C.

Steel A has the closest composition to Hudd's material and exhibits an apparent activation energy of 370 kJ mol^{-1} (Table IV). The two sets of results, therefore, are consistent.

Knowledge of the apparent activation energy of softening for a particular steel allows the equivalence between the time and temperature of annealing to be established. Accordingly, the last two columns of Table IV are calculated from the above apparent activation energies and show the softening rates of discrete temperatures relative to the rate at 660° C. For example, the same softening would be obtained in Steel A by soaking for 1 h at 715° C as by soaking for 15 h at 660° C. The use of these time–temperature equivalences enables the hardness measurements for a given steel at the various annealing temperatures to be converted to those at any single temperature. The hardness of a given steel during annealing can then be represented by a single line on a composite diagram. Fig. 3, for example, shows the hardness of all the steels plotted against equivalent hours at 660° C, which allows comparisons between steels to be readily made.

3.3. Microstructural examination

Fig. 4 shows the effects of the main variables on carbide spacing: steel composition, coiling temperature and amount of annealing. Fig. 5 gives the influence of carbon content. The greatest effect is generated by raising the coiling temperature from 600° to 750° C, when the carbide spacing is increased from 0.024 to 0.28 mm.

The above variables were also found to have a similar qualitative effect on grain size (Fig. 6). In fact, Fig. 7 indicates that there is a positive association between carbide spacing and grain size. The physical basis for this association is considered to be the inhibiting effect of carbide particles on grain boundary migration. The much larger grain size in Steel D than in A(HCT) at the same carbide spacing occurs because its lower carbon content results in the dissolution of most of its carbides at the annealing temperature.

4. Discussion

4.1. Factors contributing to softening

Rimmed steels are fully recrystallized by the time the soaking temperature is reached in commercial batch annealing furnaces, and so softening is due to microstructural coarsening. The yield strength σ_y of recrystallized rimmed steel may be expressed [4, 5] as

$$\sigma_y = \sigma_0 + \sigma_s + \sigma_G + \sigma_D \quad (3)$$

where σ_s, σ_G and σ_D are the contributions to strength from solid solution hardening, grain refinement and particle dispersion hardening respectively and σ_0 is a constant. σ_0 and σ_s are constant for a given steel and so softening during the microstuctural coarsening stage must be due to decreases in σ_G and σ_D. σ_G (N mm^{-2}) has been evaluated for annealed rimmed steel by Evans [6] as

$$\sigma_G = 19.5d^{-1/2} \quad (4)$$

where d (mm) is the grain intercept length. σ_D (N mm^{-2}) can be estimated [4, 7, 8] for ferritic steels using the Ashby–Orowan equation:

$$\sigma_D = \frac{4.45f^{1/2}}{a} \ln (3260a) \quad (5)$$

where f and a are the volume fraction and three-dimensional radius (μm) of the constituent particles respectively. $1/a$ is the dominant function of a in Equation 5 so that dispersion strengthening increases with decreasing particle size and increasing volume fraction.

Carbide particles are the main contributors to dispersion hardening in conventional rimmed steels. σ_G and σ_D can be calculated from the grain size and carbide spacing data, and are plotted along with the

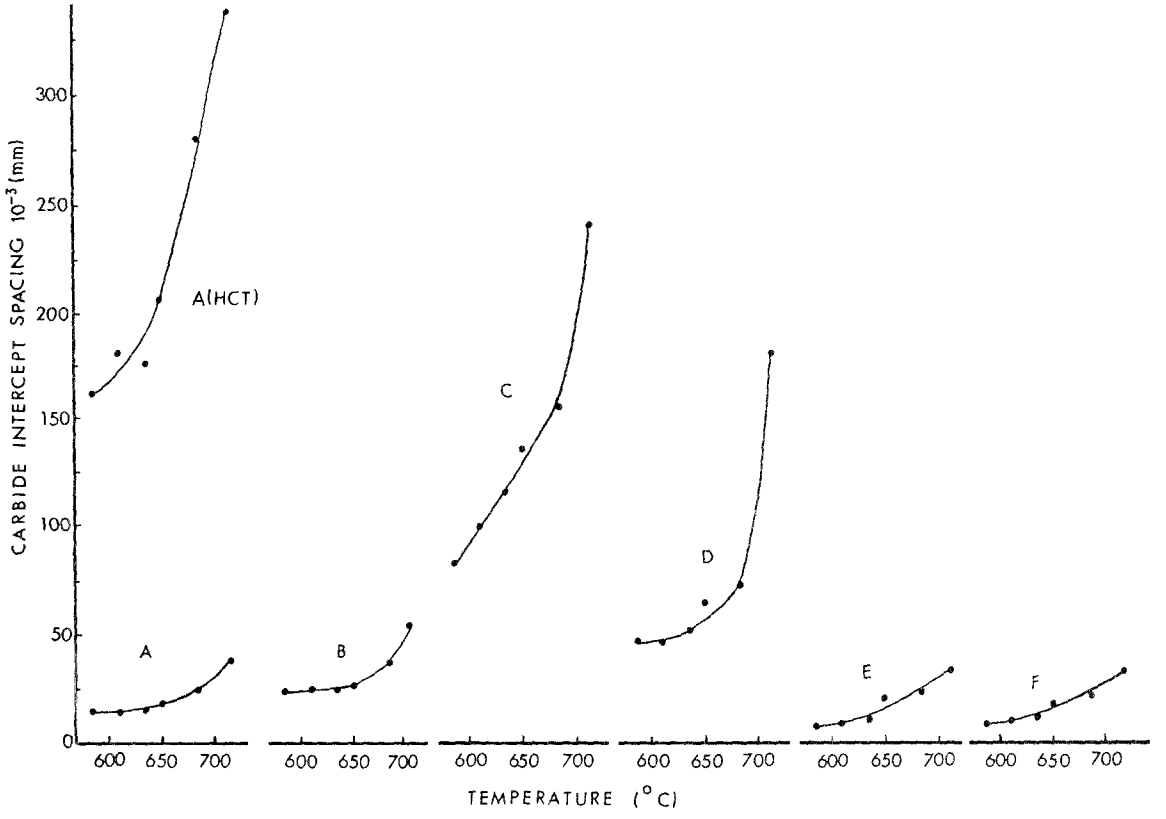

Figure 4 Carbide spacings of Steels A to F throughout annealing.

experimentally measured yield strengths σ_y for increasing amounts of annealing in Fig. 8. It is immediately clear that grain refinement (σ_G) provides a much larger contribution to the yield strength than dispersion hardening (σ_D). The decrease in σ_G throughout annealing is also substantially larger than that in σ_D. It is concluded, therefore, that grain growth produces the major contribution to softening in rimmed steels during the microstructural coarsening stage of annealing; carbide coarsening has a much smaller, but significant, effect.

4.2. Softening mechanism during annealing

The driving force for both carbide particle coarsening and grain growth stems from the resulting decrease in internal energy associated with the reduction in

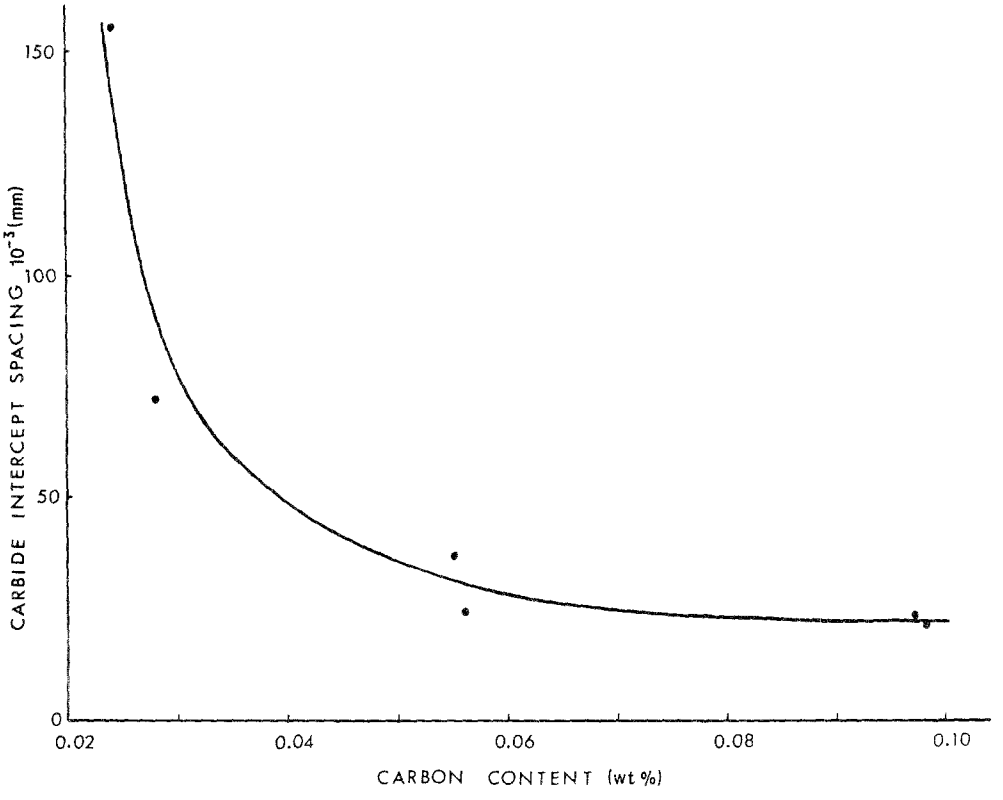

Figure 5 Carbide spacing of rimmed steels (coiled at 600° C and batch-annealed at 685° C for 26 h) against carbon content.

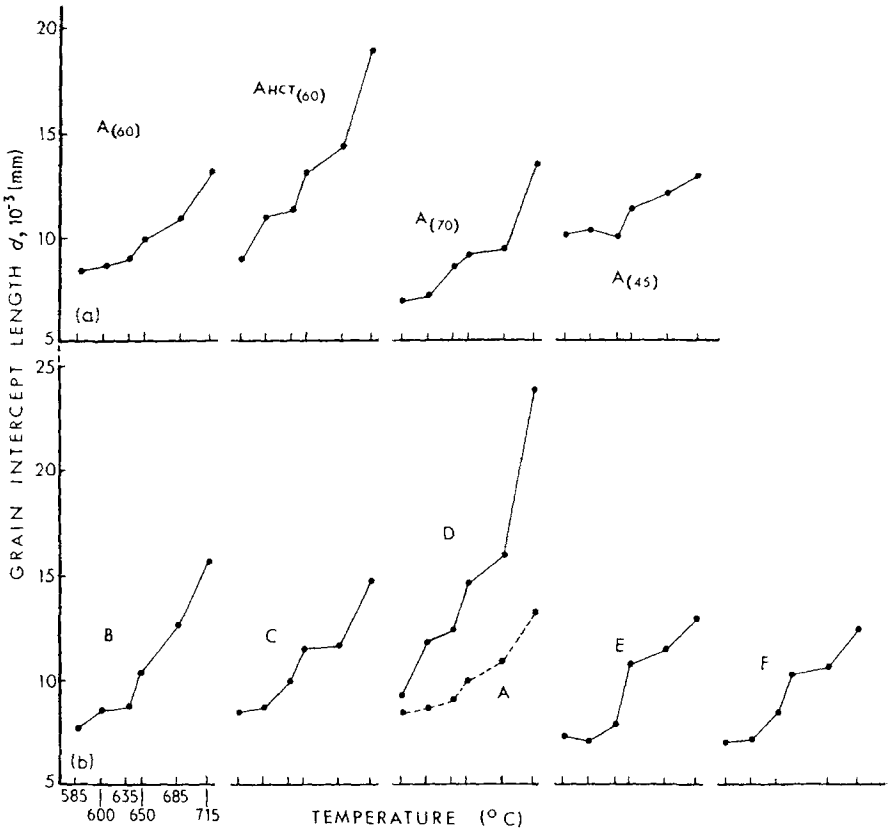

Figure 6 Effect of (a) processing and (b) composition on grain size. The same annealing treatment was given to each steel: 0.25 h at 585°, 600° and 635° C; 26 h at 650° C and 685° C; 75 h at 715° C. In (a), figures in brackets are percentage reductions. In (b), all steels were cold reduced by 60%.

interface are per unit volume. As a result, the larger particles or grains will grow at the expense of the smaller. The larger particles are surrounded by lower carbon concentrations in the matrix due to their lower surface energy than the smaller ones, which results in a net flow of carbon atoms down the concentration gradient. A relatively large grain can grow into its smaller neighbours since the expansion of its own boundary area will be more than compensated by the concurrent elimination of the grain boundary area of its neighbours [9, 10].

The present data (Fig. 7) indicate that the presence of carbide particles affects grain growth. This can take place by the pinning of grain boundaries by particles.

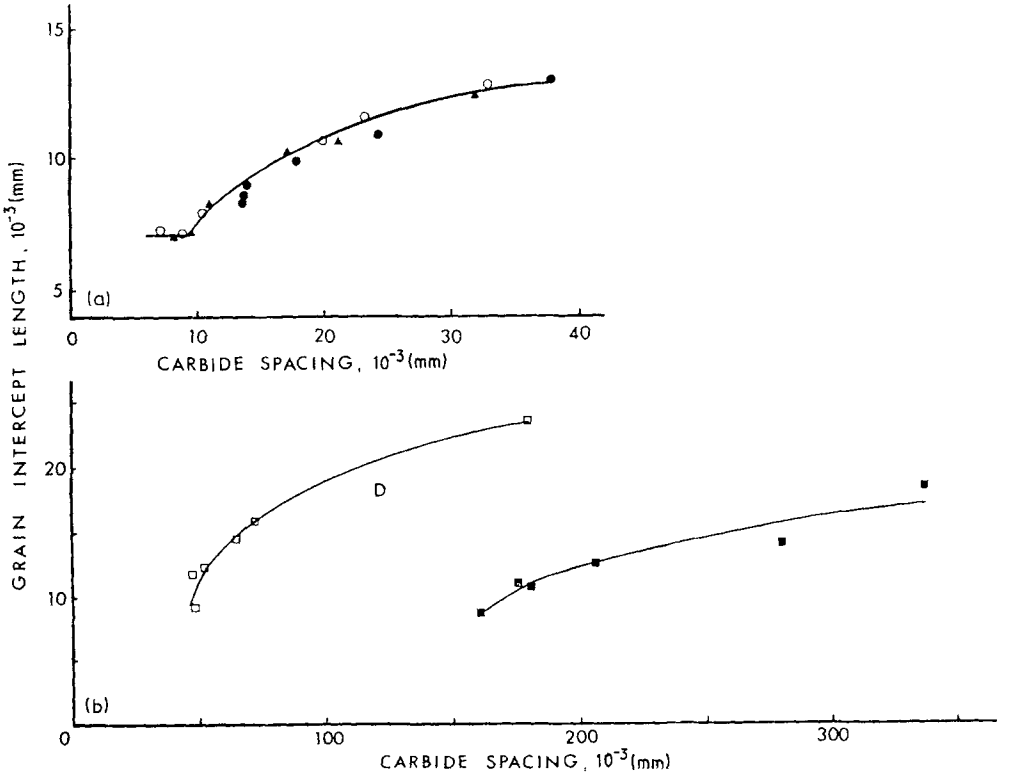

Figure 7 Grain size against carbide spacing during batch annealing of steels: (a) (●) Steel A, (○) Steel E, (▲) Steel F; (b) (□) Steel D, (■) Steel A (HCT). All steels coiled at 600° C except A(HCT), which was coiled at 750° C; all steels cold reduced by 60%. Note different scales in (a) and (b).

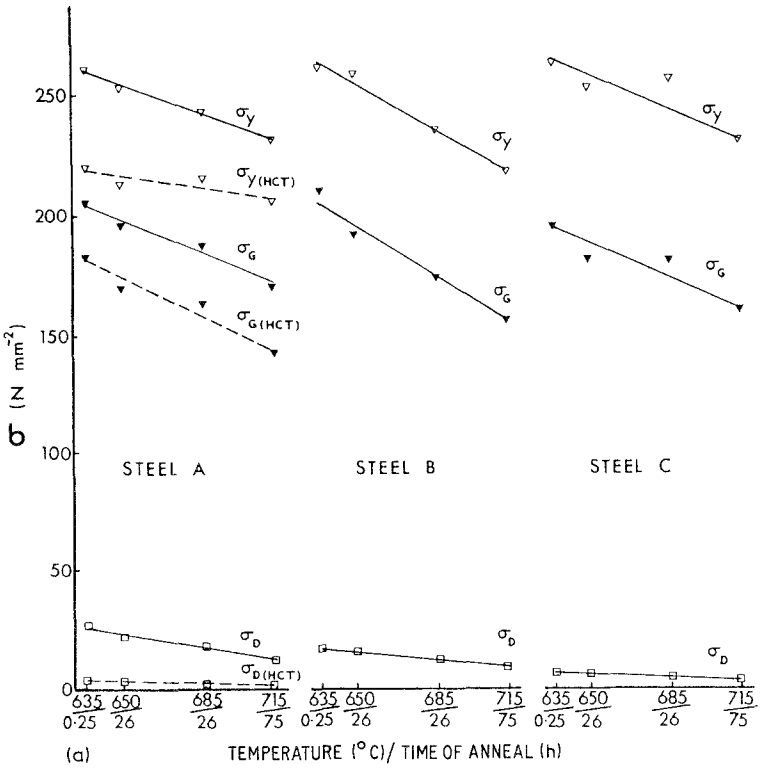

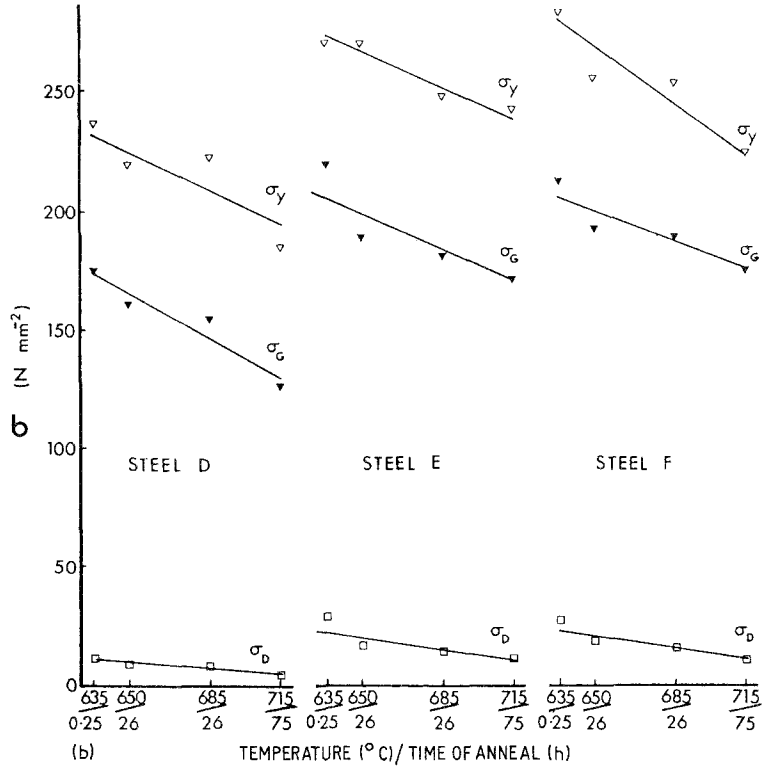

Figure 8 Contributions of grain size (σ_G) and disposition hardening (σ_D) to observed yield strength (σ_y). (a) Steels A, B and C; (b) Steels D, E and F.

The pinning effect derives mainly from the reduction in interfacial area when a grain boundary intersects a particle. The grain growth process can enable the boundary to escape from the particle by producing a sufficient energy reduction to more than compensate for the energy increment on unpinning. Zener [11] considered this retardation by a uniform dispersion of particles of radius a in terms of a particle drag per unit area Z, given by

$$Z = 3f\gamma/4a \tag{6}$$

where f is the volume fraction of dispersed particles and γ is the grain boundary energy per unit area. The radius a of the particles is related to the particle spacing x by [12]

$$a = 3fx/4 \tag{7}$$

and substituting for a in Equation 6 gives

$$Z = \gamma/x \tag{8}$$

Particle drag may be considered to reduce the driving force for grain growth; Hillert [13] and Dunn and Walter [25] have used this to derive the following equation for normal grain growth in a dispersion-bearing material:

$$\frac{dr}{dt} = \frac{M\gamma}{4r}\left(1 - \frac{Zr}{\gamma}\right)^2 \quad (9)$$

where r is the mean grain radius of the structure, t the time and M the boundary mobility. Combining Equations 8 and 9,

$$\frac{dr}{dt} = \frac{M\gamma}{4r}\left(1 - \frac{r}{x}\right)^2 \quad (10)$$

Hillert's analysis [13] can only be strictly applied when the particle drag effect is not dominating, otherwise the relative grain size distribution may change. Nevertheless, Equation 10 suggests the existence of a limiting grain radius for grain growth r_L, above which normal grain coarsening cannot take place and which is related to the particle spacing:

$$r_L \sim x \quad (11)$$

The experimental results in Fig. 7b show that grain growth in Steels D and A(HCT) commences immediately after recrystallization; this is consistent with the above reasoning since their carbide spacings are much larger than the as-recrystallized grain size. In Steels A, E and F, however, the magnitude of the carbide spacing immediately after recrystallization is close to that of the grain size and no grain growth takes place. As the temperature continues to rise, the carbide spacing increases and a stage is eventually reached when it becomes larger enough to allow grain growth to occur (as shown in Fig. 7a).

The ten-fold increase in carbide spacing from Steel A to A(HCT) is found to give only a very slight increase in the as-recrystallized grain size, whereas the latter is almost halved by increasing the cold reduction from 45 to 70% (Table III and Fig. 4). The implication is that the carbide particle drag is small compared with the driving force for recrystallization, which is likely to derive mainly from the elimination of dislocations. A steel given an appropriate cold reduction, therefore, can develop an as-recrystallized grain size much greater than its carbide spacing and thus form a stable grain structure. The driving force for grain growth is much smaller than that for recrystallization, and here the carbide dispersion exerts an important influence on grain size. It is noted that the conditions to maximize grain growth are a coarse carbide dispersion and a fine grain size. It is concluded that carbide particles affect softening indirectly by their inhibition of grain growth, in addition to their direct effect due to dispersion hardening.

4.3. Influence of composition on softening kinetics

4.3.1. Carbon

An estimate of the influence of carbon content on softening kinetics can be gained from a comparison of the data for Steels E, A and D. These materials have respective carbon levels of 0.097, 0.056 and 0.028% with no important differences in the concentrations of the other elements. The corresponding apparent activation energies of softening for these steels are 250, 370 and 490 kJ mol^{-1} (Table IV). The apparent activation energy increases, therefore, with decreasing carbon content. The softening of rimmed steels thus becomes more sensitive to temperature as the carbon content is lowered.

The solubility of carbon in ferrite increases from about 0.01% at 600° C to 0.02% at 720° C. Consequently, a significant proportion of the total carbide population will dissolve and so increase the carbide spacing as the annealing temperature is raised. This dissolution mechanism will increase the sensitivity of carbide spacing to temperature, and the magnitude of the effect will increase as the carbon content is lowered. For example, in Steel D with a carbon content of 0.028%, the carbide content is reduced from 60 to 25% of its room-temperature value as the temperature increases from 600° to 720° C. The corresponding reduction in steel E with 0.097% carbon is only from 88 to 79%. This relatively rapid change in carbide spacing with temperature will cause the grain size to become more sensitive to annealing temperature at low carbon contents, resulting in an increase in the apparent activation energy of softening. The effect will be accentuated by the tendency for carbides at grain boundaries to dissolve preferentially.

4.3.2. Manganese

The influence of manganese content on softening kinetics can be estimated from the data for Steels C and D, which contain respective manganese contents of 0.21 and 0.33% at a carbon level of 0.024 to 0.028%. Steel D possesses a relatively high apparent activation energy (490 kJ mol^{-1}, Table IV) due to its low carbon content. Steel C, however, exhibits a much lower apparent activation energy (320 kJ mol^{-1}) despite its slightly lower carbon content. The reduction in manganese content has evidently decreased the apparent activation energy of softening in these steels.

Manganese in rimmed steels exists in solid solution and combined as oxides and sulphides. In principle, manganese in solution will impede grain growth. However, the fact that raising the manganese from 0.21 to 0.33% in Steels C and D leads to an increase in the grain growth rate implies that other effects predominate. The manganese combined as oxide inclusions is too coarsely dispersed to affect grain growth significantly. Under certain circumstances, however, the manganese in the form of the sulphide is expected to precipitate as a fine dispersion. During slab reheating, a proportion of the manganese sulphide inclusions dissolve to form a solid solution of manganese and sulphur:

$$MnS = Mn + S \quad (12)$$

The equilibrium constant K for the above reaction is given by

$$K = \frac{a_{Mn}a_S}{a_{MnS}} \quad (13)$$

where a_{Mn}, a_S and a_{MnS} are the activities of manganese, sulphur and MnS. The manganese sulphide may be assumed to be sufficiently pure to give an activity of unity. The activity of manganese may be written

$$a_{Mn} = f_{Mn}Mn \quad (14)$$

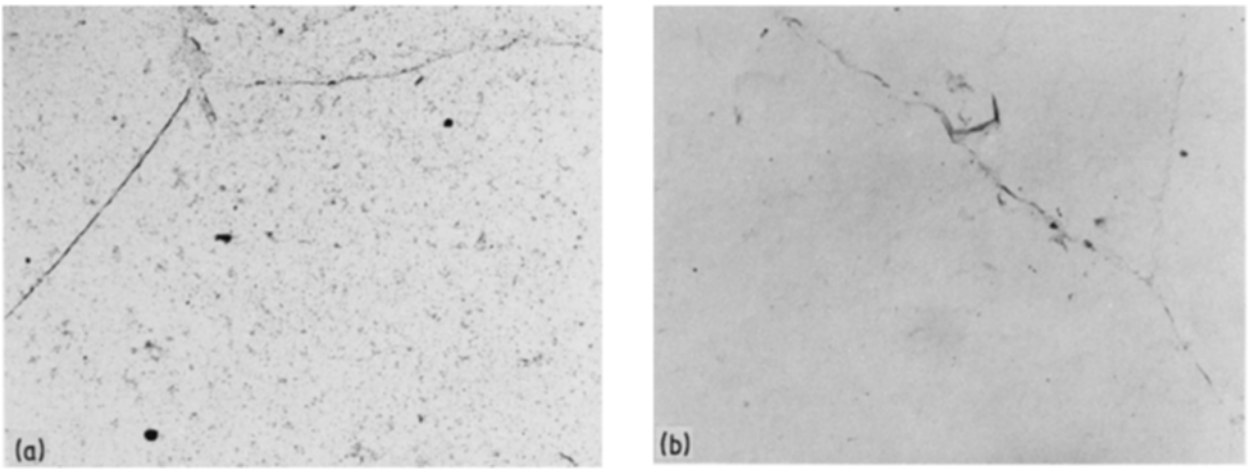

Figure 9 Electron micrographs of (a) Steel C and (b) Steel D × 12900.

where Mn is the weight percentage of available manganese in the steel (i.e. the manganese not combined as oxides and available to take part in Reaction 12) and f_{Mn} is its activity coefficient, which for these steels may be taken as unity [14]. The activity of sulphur may be expressed as

$$a_S = f_S^S f_S^{Mn} S \quad (15)$$

where S is the weight percentage of sulphur, f_S^S is the activity coefficient of sulphur in an Fe–S solid solution and f_S^{Mn} is the interaction coefficient of manganese on sulphur in an Fe–S–Mn solution. The value of f_S^S may be taken as unity, but Turkdogan *et al.* [14] found that manganese depressed the activity coefficient of sulphur such that f_S^{Mn} exhibited a value significantly below unity. However, the manganese contents of the steels in the present investigation are below those of Turkdogan *et al.* [14] and extrapolation of their data gives values of f_S^{Mn} close to unity for the current steels. Combining Equations 13, 14 and 15 and substituting values of unity for f_{Mn}, f_S^S and f_S^{Mn} gives

$$K = MnS \quad (16)$$

which may be rewritten

$$K = \left(Mn - \frac{55}{32} S_c\right)(S - S_c) \quad (17)$$

where S is the total sulphur content in weight per cent, S_c is the sulphur combined as MnS and (55/32) S_c is the corresponding manganese combined as MnS. The equilibrium constant has been evaluated experimentally [14] as

$$\log K = 2.929 - \frac{9020}{T} \quad (18)$$

where T is the absolute temperature.

Combining Equations 17 and 18,

$$\log\left(Mn - \frac{55}{32} S_c\right)(S - S_c) = 2.929 - \frac{9020}{T} \quad (19)$$

Since $Mn \gg (55/32)\, S_c$, to a first approximation

$$\log (S - S_c) = 2.929 - \frac{9020}{T} - \log Mn \quad (20)$$

Equation 20 shows that the sulphur in solution falls with decreasing temperature. During processing the steels are slab-reheated at 1300° C, hot rolled to gauge through a train of rolling stands with a finishing temperature of 900° C before spray cooling to a coiling temperature of 600° C. The relatively rapid cooling rates throughout this hot-rolling process will tend to suppress precipitation of the sulphur in solution as manganese sulphide until after coiling, when the comparatively low temperatures may be expected to generate a fine precipitate dispersion. The volume fraction of these precipitates will thus be approximately related to the sulphur in solution ($S - S_c$) at the slab-reheating temperature, since there is always a stoichiometric excess of manganese over sulphur to avoid hot shortness.

The magnitude of the sulphur in solution may be obtained from Equation 20 by substituting T = 1573 K and the appropriate value of the available manganese: Mn = (total manganese − manganese combined as oxides). The oxygen content of Steels C and D was 0.03 wt % giving 0.10 wt % Mn combined as oxides. Substitution of the values for Steel C with a total manganese content of 0.21 wt % (Table I) into Equation 20 gives 0.014 wt % S in solution and the equivalent calculation for Steel D gives a value of 0.007 wt % S in solution. These amounts of sulphur in solution are, in principle, enough to influence the final grain size providing the precipitate dispersion is sufficiently fine. In comparison, as little as 0.003 wt % N in solution, which subsequently precipitates as aluminium nitride, is known to have a drastic effect on the grain structure of aluminium-killed steels.

Equation 20 indicates that the sulphur in solution and hence the volume fraction of MnS precipitates will increase as the manganese content is reduced. Electron microscopy (Fig. 9) revealed substantially more fine precipitates in Steel C (0.21 wt % M) than in Steel D (0.33 wt % M), which is consistent with this mechanism. However, the precipitates in Steel C could not be identified and so the evidence can only be circumstantial at this stage. Nevertheless, it is suggested that the presence of a fine dispersion of MnS in Steel C is responsible for its lower grain growth rate and finer grain structure relative to Steel D. This fine

dispersion will also lessen the effect of carbide dissolution on grain growth, which may be the reason for the decrease in apparent activation of softening with decreasing manganese content.

Steels C and D contain relatively low carbon contents for rimmed steels, and at the more conventional level of 0.05% carbide dissolution will have less effect on grain growth; hence the softening kinetics will be less sensitive to manganese content. It is also noted that lowering the slab-reheating temperature will reduce the effect of manganese on softening kinetics by decreasing the sulphur taken into solution.

The influence of manganese on softening kinetics is greatest at low manganese levels, and a subtle consequence of this is to be found in the deoxidation practice during secondary steelmaking. A substantial proportion of the total manganese in rimmed steel exists as the oxide which reduces the level of manganese in solution. In killed steels, however, the oxygen preferentially combines with the deoxidant (e.g. aluminium or silicon) so that practically no manganese is lost to the oxide, and the manganese in solution will be much higher than that in a rimmed steel of the same total manganese content. The softening kinetics and properties of rimmed steel, therefore, will be more sensitive to manganese content than those of killed steels.

4.3.3. Sulphur

Steels A and B contain 0.022 and 0.039% S respectively and exhibit corresponding apparent activation energies for softening of 370 and 280 kJ mol^{-1} (Tables I and IV). Raising the sulphur content, therefore, decreases the apparent activation energy. There is a large stoichiometric excess of manganese over sulphur and so an increase in sulphur produces a corresponding increase in MnS and a decrease in manganese in solution. Increasing the sulphur content is thus expected to give a similar effect as reducing the manganese, and to decrease the apparent activation energy.

TABLE V Effect of process variables on the apparent activation energy of Steel A

Coiling temperature (C)	Cold reduction (%)	Apparent activation energy (kJ mol^{-1})
750	60	380
600	45	350
600	60	370
600	70	350

4.3.4. Nitrogen

Steels E and F contain nitrogen contents of 0.0032 and 0.0056% respectively, and corresponding apparent activation energies for softening of 250 and 280 kJ mol^{-1} (Tables I and IV). It is concluded that the normal variations in nitrogen content occurring in rimmed steel have little significant effect on the apparent activation energy.

4.4. Influence of process variables on softening kinetics

Steel A(HCT) was given a simulated coiling treatment at 750° C but still exhibited a similar apparent activation energy for softening as Steel A which was coiled at 600° C (Table IV). Samples of Steel A were also given cold reductions of 45, 60 and 70% prior to annealing but the results in Table V again show no significant variation in the apparent activation energy. Hence, the normal variations in coiling temperature and cold reduction do not affect the apparent activation energy of softening.

Fig. 10 shows the influence of process variables on hardness level. The high coiling temperature produces coarse carbides which result in a coarse grain

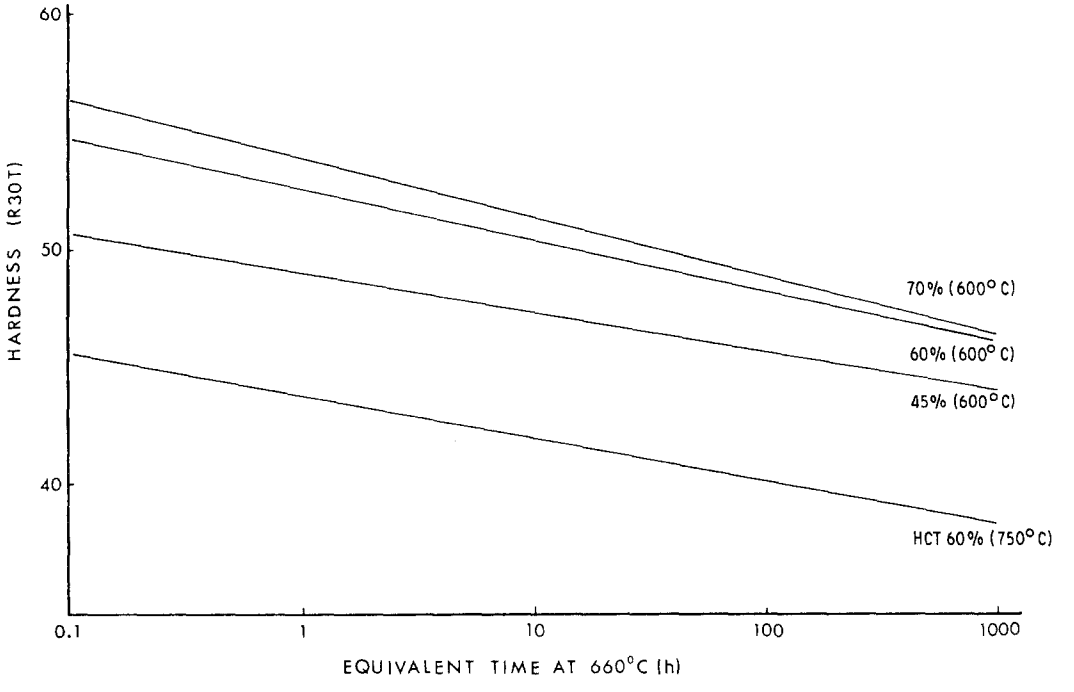

Figure 10 Effect of process variables on hardness of rimmed Steel A. Curves are labelled with the percentage reduction by cold rolling and the coiling temperature (in brackets).

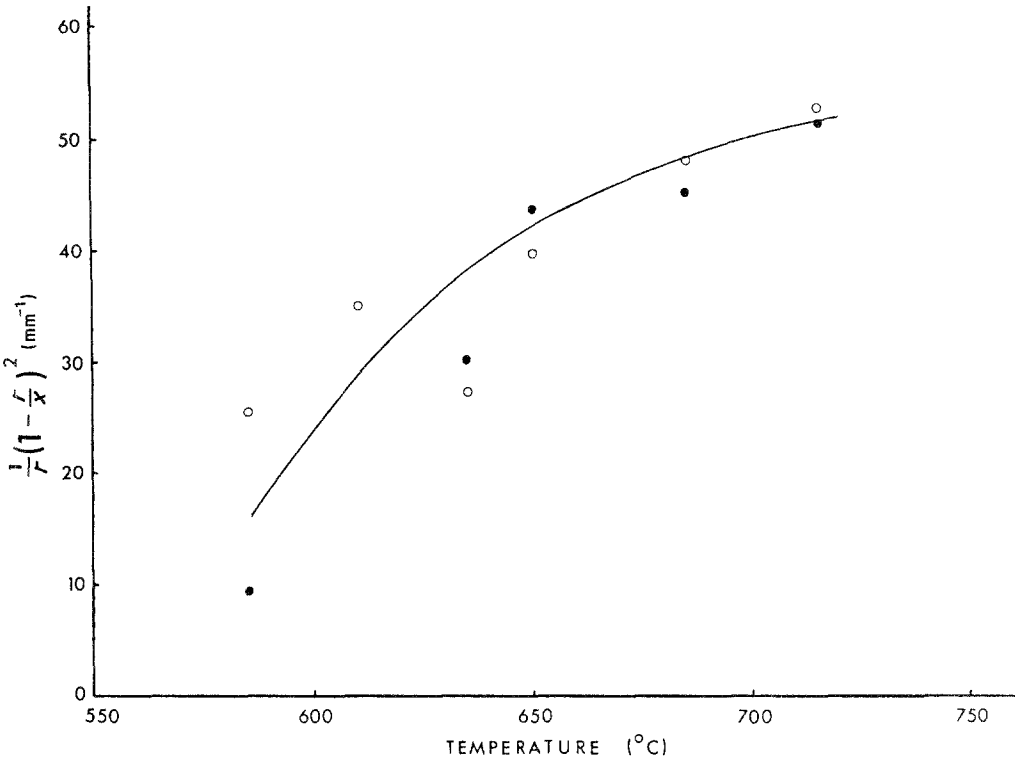

Figure 11 Grain growth factor as a function of temperature: (●) Steel E, (○) Steel F.

structure, whereas the low cold reduction gives a similar effect on grain size by a reduced nucleation rate of recrystallization.

4.5. Apparent activation energies

Softening in rimmed steels is due to carbide coarsening and grain growth. In the case of carbide coarsening, the transformation from cementite to ferrite involves an increase in density as the volume of one molecule of Fe_3C is greater than that of three atoms of iron in ferrite. This gives rise to volume constraints around particles which, in principle, can be accommodated by dislocation creation, coupled diffusion or vacancy production. The evidence in the literature [15–18] tends to discount the operation of the first two mechanisms in recrystallized ferrite, and Mukherjee *et al.* [16] conclude that the rate-controlling process for cementite coarsening in the latter material is probably the independent diffusion of vacancies to and from dislocations.

Equation 10 describes the grain growth rate in terms of grain size, carbide spacing, boundary energy and mobility. The temperature dependence of the latter term can be expressed by

$$M = M_0 \exp(-Q_m/RT) \quad (21)$$

where M_0 is a constant and Q_m the activation energy for grain-boundary migration. Substituting for M in Equation 10,

$$\frac{dr}{dt} = \frac{M_0\gamma}{4}\frac{1}{r}\left(1-\frac{r}{x}\right)^2 \exp(-Q_m/RT) \quad (22)$$

The temperature dependence of the grain growth rate will depend, therefore, on Q_m and the temperature dependence of the factor $(1/r)\,[1-(r/x)]^2$. The latter grain growth factor can be estimated [19, 20] from the data in Figs. 4 and 5 and is plotted in Fig. 11 for Steels E and F. The latter steels are considered because their high carbon and manganese contents minimize the complicating effects of carbide dissolution and fine manganese sulphide dispersions. Fig. 11 shows that the grain growth factor increases with temperature but becomes less sensitive to temperature at higher temperatures.

The physical basis for this is that the retardation of grain growth due to increasing grain size is more than compensated by the reduction in particle drag; at higher temperatures, these two conflicting effects come more into balance. The grain growth factor will increase the apparent activation energy for grain growth above Q_m; the magnitude of the increase depending upon the temperature range. This increase has a substantial influence in the range 585 to 635° C, but only a relatively small effect over the commercial soak range of 660 to 715° C. The apparent activation energy for grain growth over the commercial annealing temperature range is expected, therefore, to approximate to Q_m or self-diffusion in iron (280 kJ mol^{-1}). The apparent activation energy of softening also depends upon the fall in carbide dispersion hardening (which is directly related to carbide coarsening) as well as grain growth. However, the dispersion hardening contribution is much smaller than that from grain growth and its activation energy is in the same region as that of self-diffusion in iron. The apparent activation energy of softening, in the absence of complicating influences, is thus expected to approximate to that of self-diffusion in iron and this is consistent with the experimental results for Steels E and F (Table IV).

4.6. Practical implications

Works practices for batch annealing usually consist of allowing the coldest coil in a charge either to remain

above a specified minimum temperature for a given time or to reach a specified minimum peak temperature. The specified times and temperatures depend upon the particular grade of steel. Each steel grade has a standard annealing cycle in accordance with its property requirements. In practice, however, the tonnage and width of coils varies from charge to charge with the result that the actual time–temperature cycle given to the steel tends to deviate from the standard cycle [21–24]. For example, some charges may show unusually slow heating and cooling rates, while others may drift well above the minimum temperature or remain just below it for a considerable time. These charges will still be soaked for the standard time above the minimum temperature and so undergo much more softening than is necessary. There will be thus a distribution in the amount of annealing given to the material in a particular grade, with all parts of the frequency distribution curve above the minimum acceptable amount of annealing.

Hudd [1] has shown that a knowledge of the softening kinetics can be used to compute the softening received by a material in an arbitrary annealing cycle by integrating over the time–temperature trace as the anneal proceeds. The amount of annealing (e.g. in equivalent hours at 660° C) necessary for a particular grade can be determined from knowing the appropriate property–time relationship (e.g. Fig. 3). An anneal can then be terminated on site when the desired softening has taken place, with due allowance being made for the expected softening on subsequent cooling. In this way, unnecessary annealing is minimized and the distribution curve of annealing is sharpened with all parts still remaining above the minimum annealing condition.

The application of the above technique to the annealing of rimmed steels requires the selection of the most suitable value(s) of apparent activation energy. The latter parameter has been found to vary between 250 and 490 kJ mol^{-1}. The best value to use will depend upon the steel compositions in relation to the grade structure in a given plant. A different value of the apparent activation energy could be applied to each grade, or a single value used for all rimmed steels. In the latter case, the appropriate value may be that of the most critical grade or it may be that of the grade given the most annealing (for which the greatest savings in annealing are likely to be made). The compositional ranges of commercial grades are usually sufficiently narrow to ensure a practically constant value of the apparent activation energy of softening. The application of the technique is thus expected to generate substantial savings in throughput and energy in the annealing bay.

5. Conclusions

1. Normal variations in the compositional and process conditions of commercial rimmed steel affect the recrystallization temperature by less than 15° C.

2. Considerable softening of rimmed steel takes place after recrystallization on continued annealing due to grain growth, and to a lesser extend carbide coarsening. The carbide dispersions, however, can have an important indirect effect through their retardation of grain growth.

3. The softening kinetics of rimmed steel at commercial batch annealing temperatures can be described by an apparent activation energy. The latter parameter is strongly affected by the carbon content, varying from 490 kJ mol^{-1} at 0.025% C to 280 kJ mol^{-1} at 0.1% C.

4. The influence of carbon content on the apparent activation energy of softening is attributed to the dissolution of carbide particles during annealing. The effect is suppressed by low manganese and high sulphur contents due to the formation of fine manganese sulphide precipitates.

Acknowledgement

This work was carried out at the Welsh Laboratory, British Steel Corporation, Port Talbot and the authors wish to thank the British Steel Corporation for permission to publish the paper.

References

1. R. C. HUDD, "Steel Research 75" (British Steel Corporation, Grosvenor Place, London, 1975) p. 22.
2. D. T. GAWNE and G. T. HIGGINS, *J. Mater. Sci.* **6**, (1971) 403.
3. *Idem*, "Textures in Research and Practice" (Springer-Verlag, Berlin, 1969) p. 319.
4. D. T. GAWNE and G. M. H. LEWIS, *Mater. Sci. Technol* **1** (1985) 183.
5. *Idem, ibid.* **1** (1985) 128.
6. R. W. EVANS, *J. Iron Steel Inst.* **205** (1967) 1150.
7. T. GLADMAN, I. E. McIVOR and D. DULEIU, Proceedings of the Conference "Microalloying 75" Washington, 1975 (Union Carbide Corporation, New York, 1977) p. 32.
8. T. GLADMAN, B. HOLMES and I. D. McIVOR, "Effect of Second Phase Particles on the Mechanical Properties of Steel" (Iron and Steel Institute, Scarborough, 1971) p. 68.
9. T. GLADMAN, *Proc. R. Soc.* **294A** (1966) 298.
10. D. T. GAWNE and G. T. HIGGINS, *J. Iron Steel Inst.* **209** (1971) 562.
11. C. ZENER, *Trans. AIME* **175**, (1949) 15.
12. E. E. UNDERWOOD, "Quantitative Stereology" (Addison-Wesley, Princeton, 1970).
13. M. HILLERT, *Acta Metall.* **13** (1965) 227.
14. E. T. TURKDOGAN, S. IGNATOWICZ and J. PEARSON, *J. Iron, Steel Inst.* **180** (1955) 349.
15. R. A. ORIANI, *Acta Metall.* **12** (1964) 1399.
16. T. MUKHERJEE, W. E. STUMPF, C. M. SELLARS and W. G. M. TEGART, *J. Iron Steel Inst.* **207** (1969) 621.
17. C. LI, J. M. BLAKELY and A. H. FEINGOLD, *Acta Metall.* **14**, (1966) 1397.
18. K. M. VEDULA and R. W. HECKEL, *Met. Trans.* **1**, (1970) 9.
19. R. L. FULLMAN, *Trans. AIME* **197** (1953) 447.
20. P. L. GOLDSMITH, *Brit. J. Appl. Phys.* **18** (1967) 813.
21. G. F. HARVEY, *J. Aust. Inst. Met.* **22** (1) (1977) 28.
22. C. ROSIER, "Mathematical Models in Metallurgical Process Development", ISI Publication No. P123 (Iron and Steel Institute, London, 1970) p. 93.
23. E. A. MIZIKAR, R. A. VEITCH and N. P. BRESKY, *Industrial Heating;* **40** (a) (1973) 1608.
24. A. R. ZECCA and J. H. SCHUNK, *Iron Steel Eng.* (June 1977) 57.
25. C. G. DUNN and J. L. WALTER, in Proceedings of the Conference on Recrystallization, Grain Growth and Textures, October 1965 (American Society for Metals, Metals Park, Ohio, 1966) Ch. 10, p. 461.

Received 7 September 1984
and accepted 29 March 1985